electronics

MDPI

Article

A Buck-Boost Converter with Extended Duty-Cycle Range in the Buck Voltage Region for Renewable Energy Sources

Joaquim Monteiro [1,2,*], V. Fernão Pires [2,3], Daniel Foito [3,4], Armando Cordeiro [1,2], J. Fernando Silva [2,5] and Sónia Pinto [2,5]

1 ISEL—Instituto Superior de Engenharia de Lisboa, Instituto Politécnico de Lisboa, 1959-007 Lisboa, Portugal
2 INESC-ID, 1000-029 Lisboa, Portugal
3 SustainRD, EST Setúbal, Instituto Politécnico de Setúbal, 2914-508 Setúbal, Portugal
4 Centre of Technology and Systems (CTS-UNINOVA), 2829-516 Caparica, Portugal
5 IST—Instituto Superior Técnico, Universidade de Lisboa, 1049-001 Lisboa, Portugal
* Correspondence: joaquim.monteiro@isel.pt

Abstract: Buck-boost DC–DC converters are useful as DC grid interfaces for renewable energy resources. In the classical buck-boost converter, output voltages smaller than the input voltage (the buck region) are observed for duty cycles between 0 and 0.5. Several recent buck-boost converters have been designed to present higher voltage gains. Nevertheless, those topologies show a reduced duty-cycle range, leading to output voltages in the buck region, and thus require the use of very low duty cycles to achieve the lower range of buck output voltages. In this work, we propose a new buck-boost DC-DC converter that privileges the buck region through the extension of the duty-cycle range, enabling buck operation. In fact, the converter proposed here allows output voltages below the input voltage even with duty cycles higher than 0.6. We present the analysis, design, and testing of the extended buck-boost DC-DC converter. Several tests were conducted to illustrate the characteristics of the extended buck-boost DC-DC converter. Test results were obtained using both simulation software and a laboratory prototype.

Keywords: buck-boost; DC/DC converter; single-switch; high output voltage gain

Citation: Monteiro, J.; Pires, V.F.; Foito, D.; Cordeiro, A.; Silva, J.F.; Pinto, S. A Buck-Boost Converter with Extended Duty-Cycle Range in the Buck Voltage Region for Renewable Energy Sources. *Electronics* **2023**, *12*, 584. https://doi.org/10.3390/electronics12030584

Academic Editor: Fabio Corti

Received: 1 December 2022
Revised: 18 January 2023
Accepted: 19 January 2023
Published: 24 January 2023

1. Introduction

Currently, the use of renewable energy resources is important for decarbonization in electrical energy generation. However, many of these energy resources produce relatively low output voltages, whereas common loads require much higher loads. Customized DC-DC power converters allow the interconnection between these low-voltage resources and higher-voltage loads [1–3]. These converters can increase the penetration of renewable resources in the power grid, as well as in several applications, namely, industrial equipment, lighting, consumer electronics, and even the battery charging of electrical vehicles [4–8]. In many industrial applications, DC-DC converters stabilize the output voltage required by the load's operating conditions regardless of the input voltage variation, within reasonable limits. Some DC-DC converters have been designed [9,10] to overcome these limits and to improve their characteristics such as voltage and current ripples, power density, efficiency, and cost. DC-DC power converters have specific characteristics, and are usually selected according to the intended load requirements, such as step-down or step-up voltage gains and whether they are unidirectional or bidirectional, isolated or non-isolated, or current-fed or voltage-fed [11].

For photovoltaic (PV) energy resources or fuel cells, a DC-DC converter must offer a high step-up voltage gain, together with high efficiency in order to increase the low voltage generated by the renewable resources to a suitable utilization voltage [9,12–14]. To increase the voltage output, a step-up topology can be used, such as that in the classic DC-DC boost converter [15,16]. However, in most topologies the voltage gain is strongly limited due to

the parasitic elements of inductors, capacitors, and switching semiconductors [17]. Most conventional converters, such as the non-isolated buck-boost or the isolated push-pull system, are unacceptable as significant limitations arise from their use, for example, an extreme duty-cycle ratio, low efficiency, and poor high-frequency operation [18,19].

For applications requiring wide voltage ranges, line (low) or high-frequency transformers have been used [20,21]. However, the use of transformers introduces some issues, such as leakage inductances, parasitic capacitances, and lower efficiency due to winding and magnetic losses in the transformer [22,23]. Therefore, in order to reduce volume and weight and enhance efficiency, transformerless topologies have been devised [24–28], relying on DC-DC converters designed for high step-up voltage gains. To overcome problems related to leakage currents and human safety during maintenance routines, other solutions based on transformerless H-bridges have been proposed [29–31]. Nonetheless, these alternative solutions normally contain more power switches, increasing component counts and costs, together with increases in conduction and switching losses.

Other approaches aiming to achieve an extended voltage range have been presented to overcome the limitations imposed by the previous topologies. Most solutions employ either a specific step-up voltage technique based on multilevel boost converters [32], soft switched interleaved systems [33], cascaded DC-DC converter topologies [34], switched inductors and switched capacitor cells [35], or coupled inductor topologies [36]. Quadratic buck-boost converters, used in many applications [37], are also effective approaches to obtain high voltage gains.

Many new topologies with buck-boost characteristics have been proposed as well. Usually, converters are designed to change either the buck or the boost region ranges [38–40]. In general, these proposed designs have been engineered to increase the boost region and to obtain high boost gains. However, in these topologies, the buck region is limited to a very small range of duty-cycles. In fact, practically no studies have been conducted regarding the increasing of the buck region. Nevertheless, an increase in the buck region can be very interesting to overcome shadowing limitations in the connection of PV panels in series (PV strings), in which each panel has its own micro DC-DC converter to track the PV's maximum power operating point. Another application of micro DC-DC converters is to enforce a constant DC output voltage in grid-isolated PV panels. The output voltage of PV generator panels depends on the solar irradiance. This irradiance drops significantly when hard shadows cover some PV panels of the series-connected string, leading to significant decreases in output power for each shadowed PV. Since these panels are connected in series, as the series current of the string must be the same, the only way to harvest the highly reduced power produced by a shadowed panel is to force the micro DC-DC converter to operate within the buck region. Thus, the micro DC-DC converter proposed here may be intended to operate normally at the limits of the buck region, near the boost region. When the shadowing of some PV panels occurs, the shadowed panes go into the lower end of the buck region, whereas the non-shadowed PV panels of the series string may operate in the boost region. However, only few works have addressed this issue [41–43]. The solutions presented in these works contain relatively complex structures.

In this study, we propose a new structure for a micro buck-boost non-isolated DC-DC converter, with a single power semiconductor that favors the buck region through the enlargement of the duty-cycle range for that region. The new converter structure is suitable for applications requiring an extended buck output voltage, for example, solar PV panels with frequent shadowing conditions. Currently, in such conditions regular converters are insufficient, as their indicated sets of input voltage and/or output voltages are not sufficient for the conversion ratios needed. The structure studied here has a voltage gain feature that is extended in the buck region when compared with the classic buck-boost converter, and also features power switch and diodes with reduced voltage stresses. In this paper, a theoretical analysis and the design of this new topology are presented. To validate the converter performance, several results were obtained using simulation software and a laboratory prototype was developed and tested to obtain experimental results to match the simulation results.

2. Analysis and Principle of Operation

The well-known DC-DC buck-boost converter topology (Figure 1) is widely used in systems where the output voltage must be either higher or lower with regard to the input voltage V_i [7]. One of the main applications of this kind of converter is in PV generators operating in frequently shadowed or snowy conditions. However, both the output power and voltage of PV panels present important variations since they are functions of the irradiance [44–48]. When a PV panel is shadowed, the voltage will decrease, whereas the produced power will sharply drop due to the reduced saturation current. Consequently, the PV-panel-connected converter must change the operating region, changing the voltage gain and extracted power. In series-connected strings of PV panels, as the series current is the same, the converter is forced to operate either in the buck or in the boost region to compensate for the lower power or the lower voltage. Thus, the micro DC-DC converter proposed here was designed to operate mainly in the extended buck region, although when required due to voltage drops, the converter can function in the boost region. As shown in Figure 1 and considering all components as ideal and operating in continuous conduction mode (CCM), the converter output voltage, denoted as V_o in (1), can range from 0 to infinity, for a duty cycle, δ, with a variation between 0 and 1.

$$V_o = \frac{\delta}{1-\delta} V_i \tag{1}$$

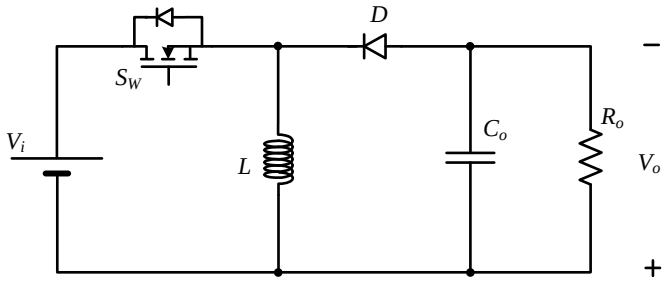

Figure 1. Conventional DC-DC buck-boost converter.

To extend the duty-cycle range for operation in the buck output voltage region, a new buck-boost micro DC-DC power converter topology is proposed here (Figure 2). Compared to typical buck-boost topologies, the new topology maintains the boost inductor and only needs a single active switch, S_w. Nevertheless, the new proposed converter features an extended output voltage static gain in the buck region when compared to conventional buck-boost converters.

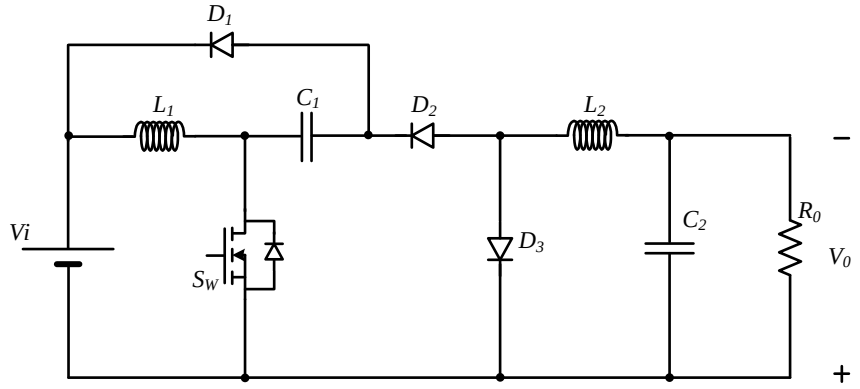

Figure 2. Extended-buck DC-DC converter with extended duty cycle in the output voltage buck region.

PV panels must track the maximum power point (MPP) with very small deviations (ripple) around this MPP. To minimize the switching ripple, for a given set of inductors and

capacitors, most DC-DC converters must operate in CCM. Therefore, in CCM an analysis of the extended-buck DC-DC converter reveals two main operation modes, as shown in Figure 3. Considering all components as ideal, with δ being the duty-cycle and T_s being the switching period, the following two operation modes can be described:

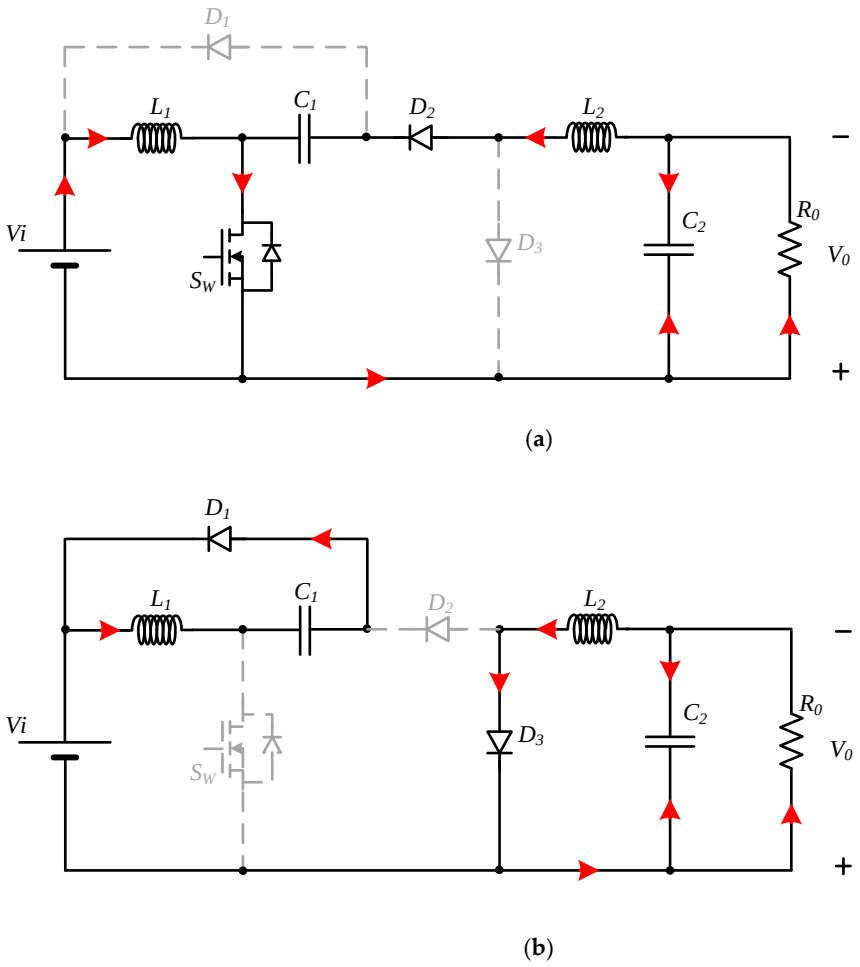

Figure 3. Converter operation modes. (**a**) Mode 1—S_w is ON. (**b**) Mode 2—S_w is OFF.

Operation mode 1, S_w *is driven ON*: during the time interval from 0 to δT_s, the switch S_w is in the ON state, and diode D_2 is in the ON state, whereas diodes D_1 and D_3 are reverse-biased. The stored energy in L_1 and L_2 inductors will increase while capacitor C_1 is discharging. Consequently, the L_1 inductor current will increase and the capacitor voltage C_1 will decrease. The diode D_1 is reverse-biased as it has a negative voltage from the cathode to the anode, given by the sum of the input voltage source and the capacitor C_1 ($-V_1$- V_{C1}). Similarly, the diode D_3 is reverse-biased by the capacitor C_1.

Operation mode 2, S_w *is driven OFF*: during the time interval $(1\text{-}T_s)\delta$, the switch S_w is in the OFF state, whereas diodes D_1, D_2 and D_3 are in the ON state. The stored energy of the inductor L_1 is transmitted to the capacitor C_1. Consequently, the current of the inductor L_1 will decrease and the voltage of the capacitor C_1 will increase.

Analysis in CCM

To obtain the steady-state voltage gain of the extended-buck DC-DC converter, operation at a steady state in CCM was considered, together with ideal components. In a steady state, the L_1 and L_2 inductors' averaged voltages, V_{L1} and V_{L2}, are zero over a switching

period. Considering the two operating modes depicted in Figure 3, the averaged voltages of both inductors, as a function of the duty cycle δ, are given by the following relationships:

$$V_{L1} = \delta V_i + (1-\delta)V_{C1} = 0 \tag{2}$$

$$V_{L2} = \delta(V_0 - V_{C1}) + (1-\delta)V_0 = 0 \tag{3}$$

The output voltage gain is obtained by solving the previous equations to obtain the output voltage V_0, which is dependent on the input voltage V_i and δ.

$$V_0 = \frac{\delta^2}{1-\delta} V_i \tag{4}$$

With the previous expression, it is possible to verify that the output voltage can range from zero volts to infinity, with an extend duty-cycle range of $\delta \in (0, (\sqrt{5}-1)/2)$ in the buck region. The same conclusion can be obtained from Figure 4, in which the static voltage gain V_0/V_i is shown as a function of the duty cycle δ. The extended-buck DC-DC converter gives voltages in the buck region roughly from $\delta \approx 0$ up to $\delta \approx 0.62$, therefore extending the buck region from $\delta \approx 0.5$ (in the conventional buck-boost system) to $\delta \approx 0.62$.

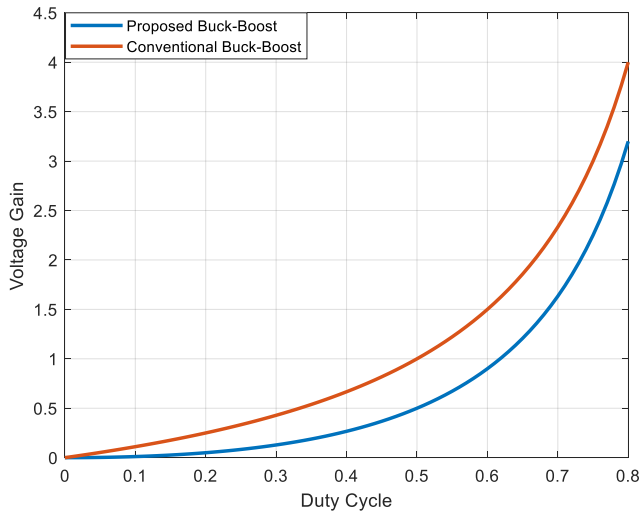

Figure 4. Voltage gains for the conventional and the extended buck region buck-boost systems.

According to (4), the theoretical voltage gain can be infinite (for a duty cycle of one); in reality, due to the non-idealities of the converter, the boost gain is bounded to a value not exceeding five. Although the proposed converter presents a wider buck range, regarding conventional topologies, it also presents a slightly lower maximum boost gain. This lower boost gain will not impair its application as a PV panel micro DC-DC converter, provided that the number of series panels allow for the operation of each panel to occur mainly in the buck region.

3. Analysis and Design of the Extended-Buck DC-DC Converter

3.1. Inductor and Capacitor Design

The inductances and capacitances of the power converter have been designed to ensure that relatively small ripples occur in the converter currents and voltages. Thus, the L_1 inductance value is calculated to guarantee a given peak-to-peak current ripple ΔI_{L1}, which should be relatively small compared to the average value of I_{L1} in a period $1/f$.

Assuming the switch-ON time and V_i as the voltage across the inductor, the L_1 inductance is a function of the current ripple ΔI_{L1}, as stated in (5).

$$L_1 = \frac{\delta V_i}{\Delta I_{L1} f} \tag{5}$$

The self-inductance of L_2 can be obtained using the previous method, equaling the current ripple ΔI_{L2} when the power switch is OFF. The self-inductance of L_2 is defined in (6).

$$L_2 = \frac{V_{C1}(1-\delta)}{\Delta I_{L2} f} \tag{6}$$

A similar procedure was used in the sizing of the capacitor C_1 of the extended-buck DC-DC converter. Considering a small voltage ripple (regarding the average voltage of the capacitor C_1) ΔV_{C1}, with a small enough equivalent series resistance and the capacitor discharge time Δt_1, as function of the duty-cycle δ, and using V_o and P_o to denote the load voltage and power, respectively, expression (7) can be obtained to determine C_1.

$$C_1 = \frac{\Delta Q}{\Delta V_{C1}} = \frac{\Delta I_{L2}}{8 \Delta V_{C1} f} \tag{7}$$

To determine the value of capacitor C_2, we assumed that its charge variation ΔQ was due to its current ripple ΔI_{L2}.

$$C_2 = \frac{1}{\Delta V_{C2}} \frac{P_o}{V_o} \Delta t_1 \tag{8}$$

From the point of view of the sizing of the components, under the same assumptions, this converter obeys relations similar to those of the Cuk converter.

3.2. Semiconductor Voltage and Current Stress

The voltage stress (V_s) across the power switch S_w is obtained via the analysis of the circuit in a steady state and considering that this voltage equals the peak voltage of the capacitor C_1. Based on these assumptions and assuming that the capacitor C_1 has a voltage ripple ΔV_{C1} and average value V_{C1}, the voltage at the power terminals of the switch when it is open is given by:

$$V_S = V_{C1} + \frac{\Delta V_{C1}}{2} \tag{9}$$

The voltage rating of the diode D_1 is equal to the voltage across the power switch S_w in the OFF state. It must be noted that, according to Figure 3a,b, the voltage across the switch and diode D_1 is given by the mesh, which is given by the input voltage source V_i, the switch S_w, the capacitor C_1, and the diode D_1. The voltage rating of the diode D_2 is given by the input source voltage V_i. In Figure 3b it can be seen that when D_1 and D_3 are ON the input source voltage is directly applied to D_2. Regarding the voltage rating of the diode D_3, it is a function of the voltage of the capacitor C_1. When D_3 is in the OFF mode (Figure 3a) and the switch S_w is ON the capacitor C_1 is directly applied to this diode. The voltage across the capacitor C_1 can be obtained from Equation (2), and is expressed in (10). Thus, the voltage ratings of both diodes (D_2 and D_3) are given in (11).

$$V_{C1} = \frac{\delta}{1-\delta} V_i \tag{10}$$

$$\begin{cases} V_{D2} = V_i \\ V_{D3} = V_{C1} \end{cases} \tag{11}$$

The current stress of the power switch S_w is a function of the load current and the duty cycle as given in (12). The load current I_o can be determined based on the nominal power

of the converter and the operation voltage value of the output DC/DC converter, assuming a conservative conversion.

$$I_{Sw} = \frac{\delta^2 I_0}{1-\delta} \tag{12}$$

These expressions enable the choice of relatively low-voltage, high-current MOSFET transistor devices in the intended applications.

3.3. Comparative Study

In this section, a comparison between the characteristics of the proposed converter and those of other similar topologies is presented in Table 1. Recent topologies available in the literature were considered [37,40–48]. Analyzing buck-boost topologies, and the number of components used in each of the compared topologies, it can be seen that the micro DC-DC converter proposed here was one of the topologies that required the minimum number of switches and other components (with the exception of the classic buck-boost topology). The proposed topology requires only one switching device, which contributes to the reduction of switching losses. The proposed topology extends the voltage gain in the buck region from $\delta \approx 0$ up to $\delta \approx 0.62$. The topologies presented in [37,48] exhibited a reduction in the buck region, but that presented in [41] exhibited an increase similar to that of the design proposed here. However, that topology with an extended buck region requires more than one switch and more passive components.

Table 1. Comparison of the proposed solution with other buck-boost topologies presented in the literature.

Items \ Topologies	Classic	[37]	[41]	[48]	Proposed
Voltage gain	$\frac{V_0}{V_i} = \frac{\delta}{1-\delta}$	$\frac{V_0}{V_i} = \frac{2\delta-\delta^2}{1-\delta}$	$\frac{V_0}{V_i} = \frac{\delta}{2(1-\delta)}$	$\frac{V_0}{V_i} = \frac{2\delta}{(1-\delta)}$	$\frac{V_0}{V_i} = \frac{\delta^2}{1-\delta}$
Buck range	0.50	0.38	0.66	0.25	0.62
Number of switches	1	1	2	3	1
Number of diodes	1	3	5	2	3
Number of inductors	1	2	2	2	2
Number of capacitors	1	2	3	1	2

4. Simulation Results

The behavior of the extended buck DC-DC converter was analyzed on the basis of numerical results obtained using the *Power Systems Toolbox* in *Matlab/Simulink* software. In the simulation tests, the component values used for the extended buck DC-DC converter were as follows: inductors L_1 = 10 mH and L_2 = 10 mH, capacitors C_1 = 20 µF and C_2 = 100 µF, obtained via the previous equations using a switching frequency of 10 kHz. The following figures were obtained in buck and boost mode.

The results presented in Figures 5–8 show the simulated waveforms for the converter in a steady state in buck mode with a duty cycle of 0.5. Figure 5 shows that the input voltage was equal to 100 V and the corresponding absolute value of the output voltage was equal to 50 V. This results showed an output voltage with an absolute value that was half of that of the input voltage, according to the voltage static gain expression (4).

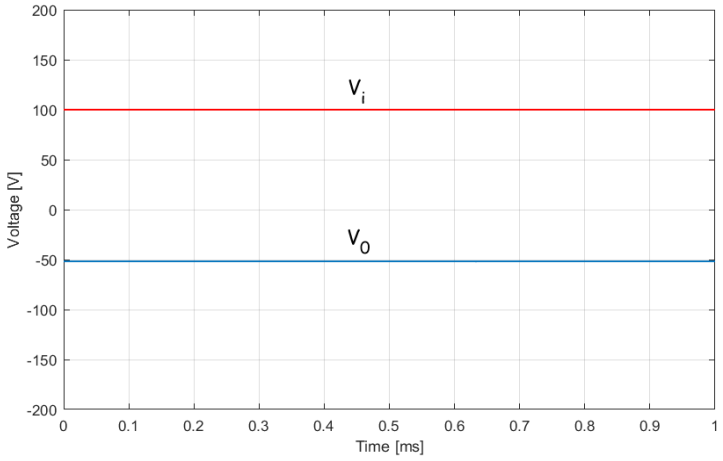

Figure 5. Simulation results of the input and inverted output voltage in buck mode.

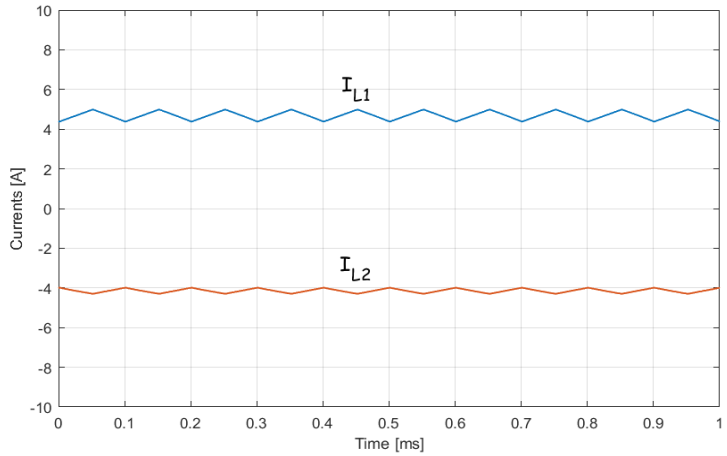

Figure 6. Simulation results of the L_1 and L_2 inductor currents in buck mode.

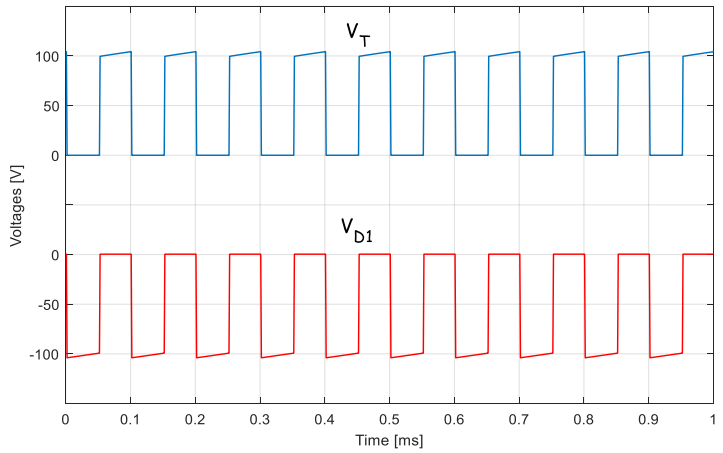

Figure 7. Simulation results of the voltage across the power switch S_W and the diode D_1 in buck mode.

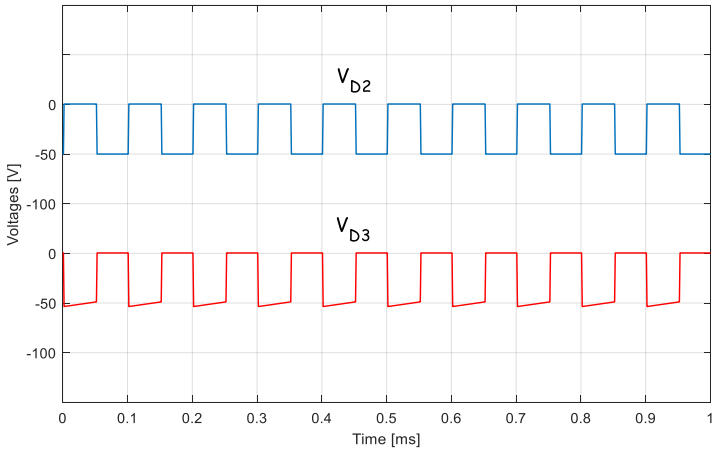

Figure 8. Simulation results of the voltage across the diodes D_2 and D_3 in buck mode.

Figure 6 shows the simulation results of the L_1 and L_2 inductor currents in buck mode. Based on these waveforms, it is possible to observe the continuous conduction mode in both inductors, with relatively small current ripples compared to the average value. The ripple of the current in inductor L_2 was smaller than the ripple in inductor L_1, as this inductor was connected to the capacitor C_2.

The voltages across the power switch and the diode D_1 are shown in Figure 7. Figure 8 shows voltages across the diodes D_2 and D_3. Based on these last waveforms, it can be observed that diodes D_2 and D_3 were working in complementary operating states. When comparing these results with the voltages on the power switch and on the diode D_1 (Figure 7), it can be seen that the D_1 reverse voltage, in terms of its absolute value, doubled the corresponding values in diodes D_2 and D_3.

The results presented in Figures 9–12 show the waveforms for the converter in a steady state in boost mode operation, with a duty-cycle of 0.7. In Figure 9, the input voltage is close to 100 V, and the corresponding output voltage approximately equals 165 V, confirming the boost mode and the theorical expectations.

Figure 10 shows the simulation results of the L_1 and L_2 inductor currents in boost mode. In this situation, it can also be seen that the CCM operation was preserved. The voltage across the power semiconductors is presented in Figures 11 and 12, confirming the expected characteristics of the boost operating mode.

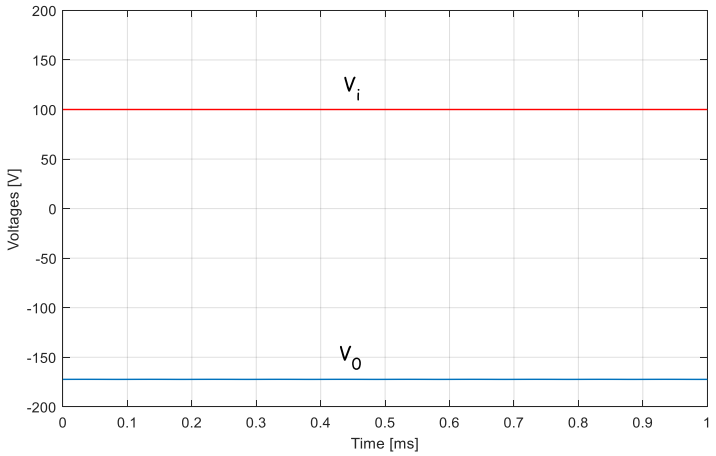

Figure 9. Simulation results of the input and inverted output voltage in boost mode.

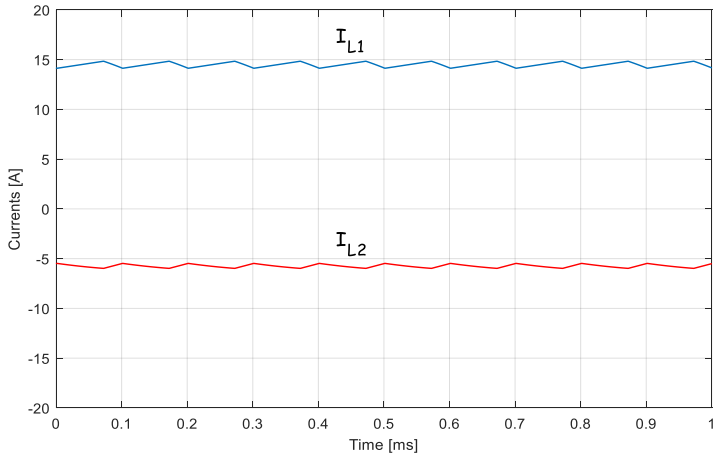

Figure 10. Simulation results of the L_1 and L_2 inductor currents in boost mode.

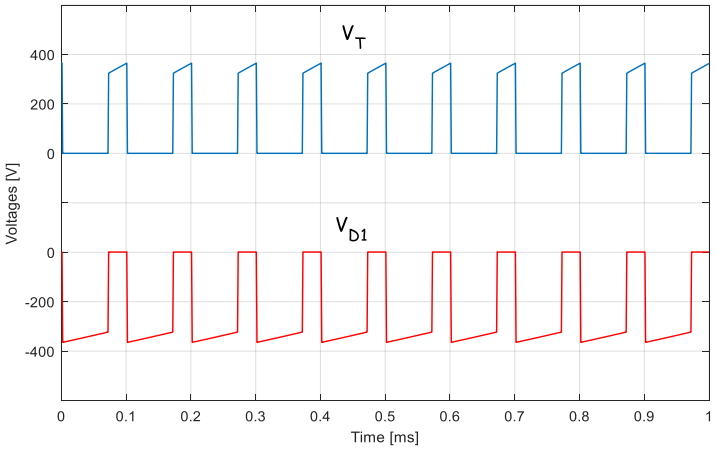

Figure 11. Simulation results of the voltage across the power switch S_W and the diode D_1 in boost mode.

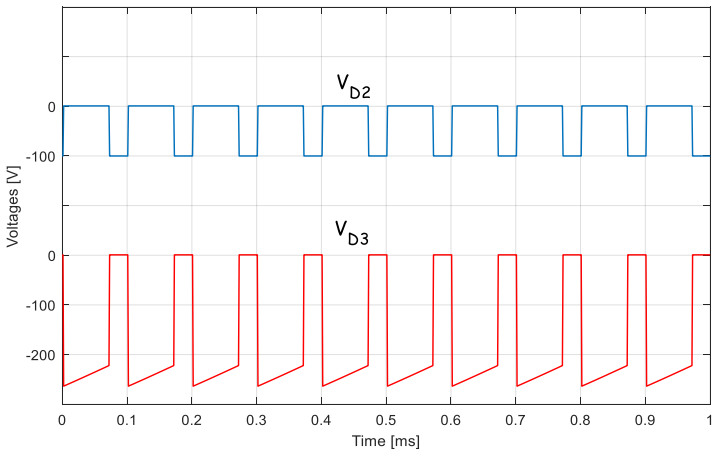

Figure 12. Simulation results of the voltage across the diodes D_2 and D_3 in boost mode.

To test the performance of the extended buck DC-DC converter, some results were obtained in dynamic conditions. The results presented in Figure 13 were obtained considering a change in the input voltage from 100 V to 70 V at the instant t = 0.2 s. Since this input voltage decreases, the output voltage also decreases (in absolute value). However, to recover the previous output voltage, at instant t = 0.48 s, the value of the duty cycle was increased, and this effect is clearly visible in Figure 13.

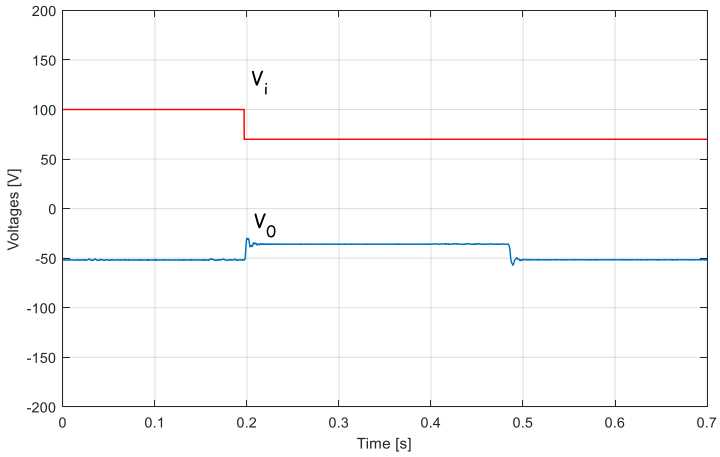

Figure 13. Simulation results of the input and inverted output voltage in transient mode.

Through the analysis of these results, it is possible to verify that when there is a sudden variation in the input voltage, the output voltage suffers a disturbance. However, the original value can be restored. Based on this result, it is possible to conclude that the micro DC-DC converter responds in accordance with the changes in the input voltages.

Another transient test was conducted, in this case taking into consideration the converter operating as a PV generator to maintain the output voltage. When the PV panel is shadowed, its output voltage decreases. Thus, at t = 0.2 s the input voltage suddenly drops from 100 V to 30 V, whereas at t = 0.45 s it recovers to the initial voltage value under shadowless conditions. To maintain the output voltage, the duty cycle has to be changed. Figure 14 presents the corresponding simulation results, where the input voltage suffered from the abovementioned voltage drop but the output voltage was maintained, except for fast and small transients. In this test, the micro DC-DC converter initially operated in the buck region, but changed to the boost region during the voltage drop in order to maintain the desired output voltage. As shown in this figure, the converter still operates properly, even during the transition between buck and boost regions.

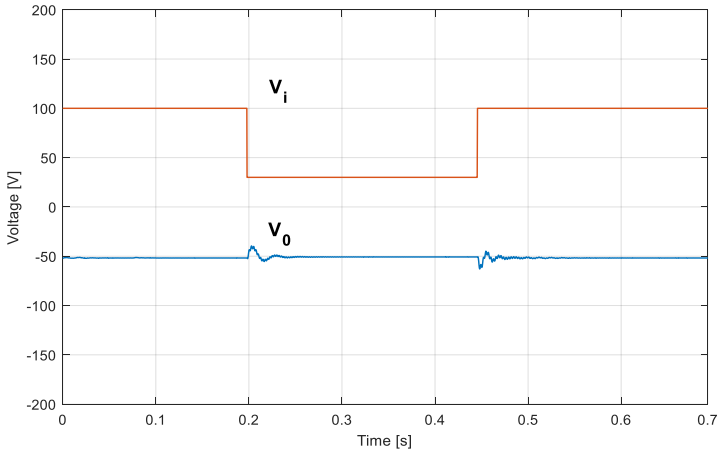

Figure 14. Simulation results of the input and output voltage in transient mode considering this converter operating with a PV system.

A comparative study regarding the efficiency of the proposed micro DC-DC converter and classic buck-boost converters was conducted. The study included the two operating modes, with the converters operating in buck mode and then operating in boost mode. Table 2 shows the tested converter results. It can be seen that the efficiency of the proposed topology was similar to that of the SEPIC topology, with almost the same values. In the boost region, the efficiency of the proposed micro DC-DC converter almost attained the

efficiency of the classic converters, with a decrease in efficiency of less than 0.5%. Solely in the buck region, the proposed micro DC-DC converter may present efficiencies 2% lower (at most) than classic converters.

Table 2. Efficiency of the proposed topology compared to some other buck-boost converters.

Buck-Boost		**Cuk**		**SEPIC**		**Proposed**	
Buck	Boost	Buck	Boost	Buck	Boost	Buck	Boost
93.7%	97.5%	94.1%	97.6%	92.8%	97.3%	92.2%	97.1%

5. Experimental Results

To validate the theorical analysis and the previous simulation results obtained for the extended buck DC-DC converter, a laboratory prototype was built using the same parameters that were used for the numerical tests. To analyze the performance of the laboratory prototype, tests were performed with the prototype under the same conditions as those of the simulation results. Figure 15 presents the experimental laboratory setup used to obtain the results presented below. In this figure, the components are labeled as follows: 1—drive circuit board; 2—micro DC-DC converter.; 3—inductors; 4—current probes; 5—resistive load; 6—waveform signal generator; 7—auxiliary DC power supply; 8—Yokogawa DL1540 oscilloscope; 9—main DC power supply. The proposed micro DC-DC converter was based on a MOSFETs ZFET 1 × 20A IDS transistor and FFSP2065B diodes.

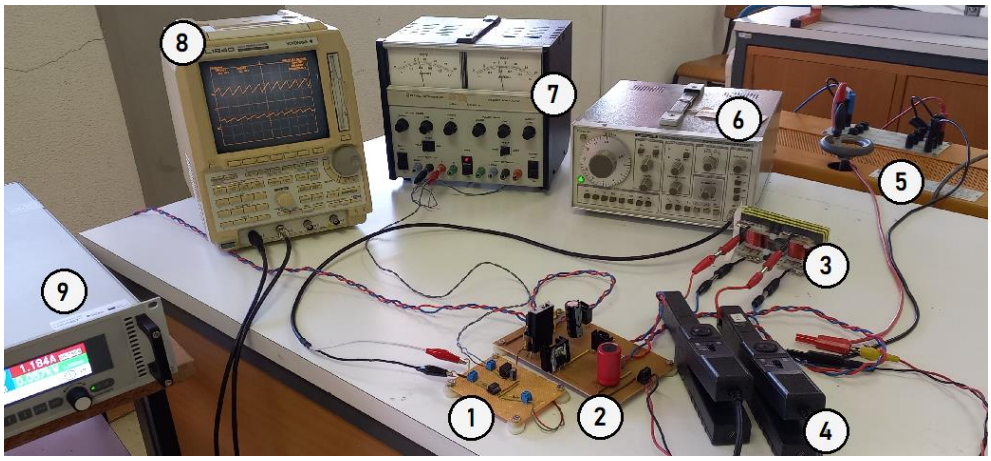

Figure 15. Experimental setup.

Figures 16–19 show the experimental results for the converter in a steady state, operating in buck mode, with a fixed duty cycle of 0.5 and a switching frequency f of 10 kHz. In Figure 16 it can be seen that the absolute value of the output voltage was half of the input voltage, according the voltage gain obtained in (4).

The experiment results for the inductor currents, I_{L1} and I_{L2}, are shown in Figure 17. These waveforms show the continuous conduction mode in both inductors and the smaller current ripple in I_{L2} with regard to I_{L1}.

Figure 18 shows the experimental result obtained for the voltages across the power switch and the diode D_1. Figure 18 depicts the experimental results for the voltages across the diodes D_2 and D_3. From these results, it is possible to observe that the diodes D_2 and D_3 were working in complementary operating states, as seen in the simulations and as expected based on the theoretical analysis.

Figures 20–24 show the experimental results for the converter in a steady state, operating in boost mode, with a duty cycle of 0.7 and a switching frequency of 10 kHz. Based on the waveforms presented in Figure 20, the voltage static gain can be seen to exceed unity.

Based on the experimental results presented in Figure 21, it can be confirmed that the currents through both inductors were in continuous mode. On the other hand, it is possible to verify that the maximum voltage across the power switch was in phase opposition and with the same absolute value as that of the voltage on the diode D_1 (Figure 22). Comparing these results with the experimental results obtained for the voltage across diodes D_2 and D_3, presented in Figure 23, it is possible to verify that the voltage across these diodes, in terms of its absolute value, was half of the voltage across S_w and D_1.

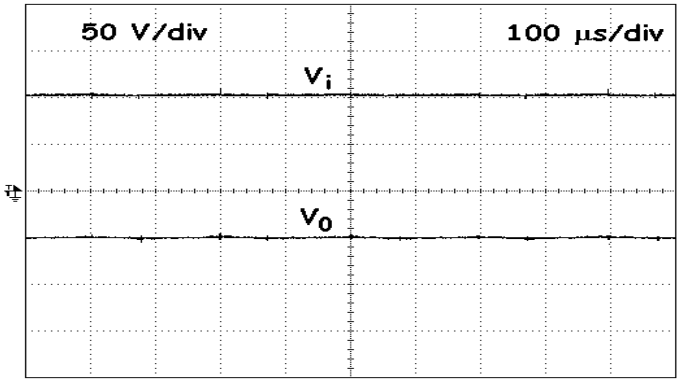

Figure 16. Experimental results for the input and inverted output voltage in buck mode.

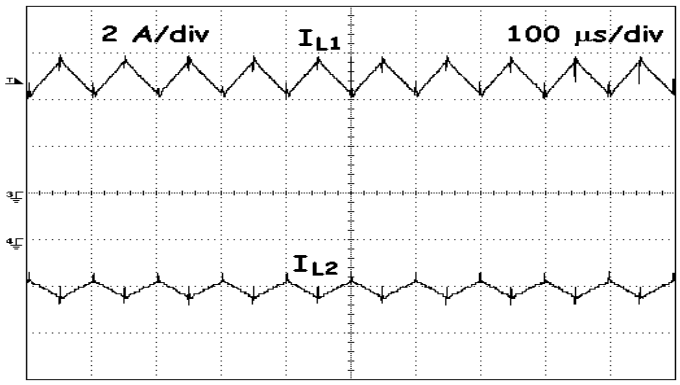

Figure 17. Experimental results for the L_1 and L_2 inductor currents in buck mode.

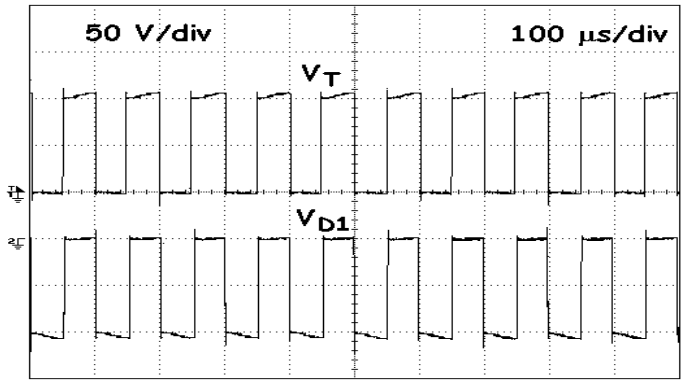

Figure 18. Experimental results for the voltage across the power switch S_W and the diode D_1 in buck mode.

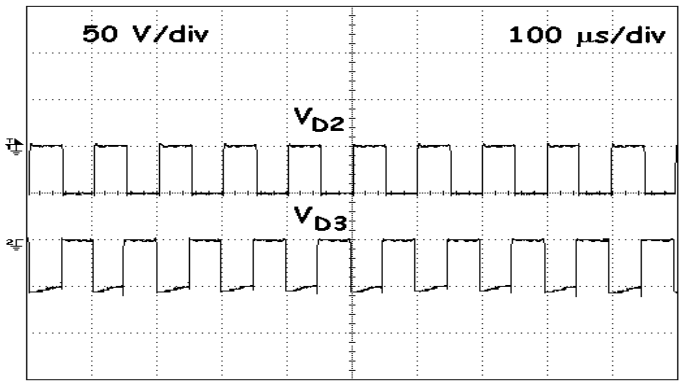

Figure 19. Experimental results for the voltage across the diodes D_2 and D_3 in buck mode.

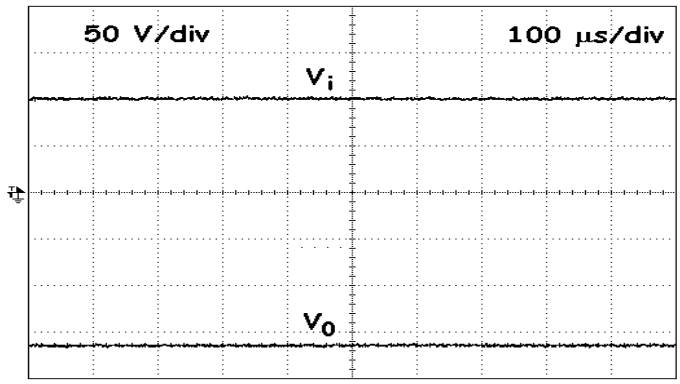

Figure 20. Experimental results for the input and inverted output voltage in boost mode (0.7).

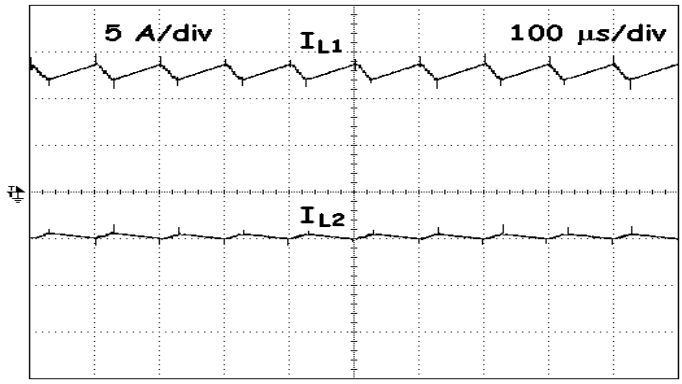

Figure 21. Experimental results for the voltage across the power switch S_W in boost mode.

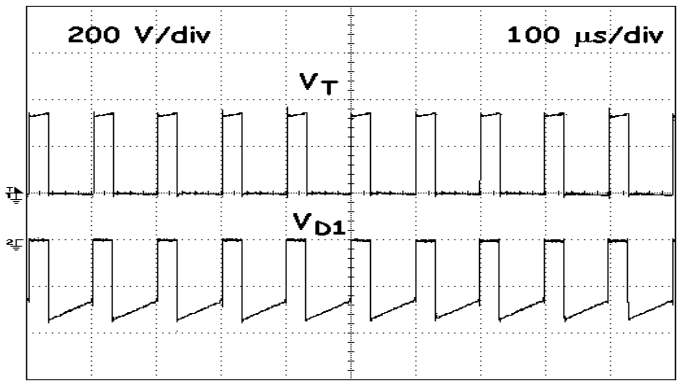

Figure 22. Experimental results for the voltage across the power switch S_W and the diode D_1 in boost mode.

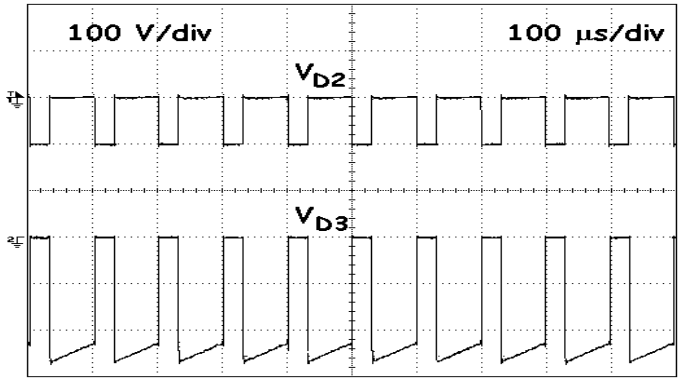

Figure 23. Experimental results for the voltage across the diodes D_2 and D_3 in boost mode.

In the laboratory experiments, results were obtained under dynamic conditions in order to test the performance of the extended-buck DC-DC converter. The results presented in Figure 24 were obtained considering a change in the input voltage from 100 V to 70 V at time t = 0.3 s. As in the simulations, in the laboratory tests, in order to recover the previous output voltage, at instant t = 0.48 s the value of the duty cycle was increased, with this effect being clearly visible in Figure 24. This shows that sudden variation in the input voltage causes a disturbance in the output voltage, but this disturbance can be mitigated by changing the duty cycle.

However, to visualize the impact of this converter in a PV system operating under shadow conditions, further transient results are presented in Figure 25. In this case, the input voltage decreases and after a while returns to the normal value. To maintain the output voltage, the duty cycle was changed. In this case, the change occurred from the buck region to the boost region and back to the buck region. It is thus possible to ensure proper operation even when there are changes in those two regions, in spite of the presence of brief and small transients.

The efficiency of the proposed micro DC-DC converter as a function of the output power was measured, with the obtained results plotted in Figure 26. The blue curve shows the efficiency in buck mode (with a duty cycle equal to 0.5), whereas the red curve shows the efficiency in boost mode (with a duty cycle equal to 0.7). Although at low power the efficiency of these two modes was similar, at higher power the efficiency of the converter in boost mode increased.

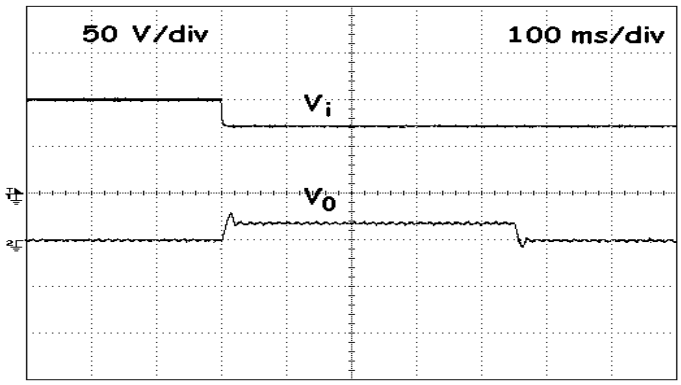

Figure 24. Experimental results for the input and output voltage in transient mode.

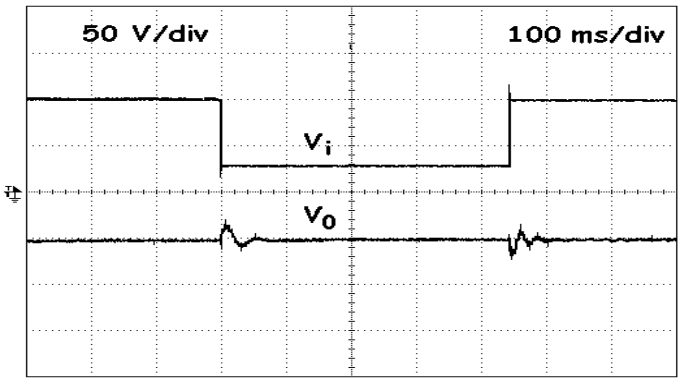

Figure 25. Experimental results for the input and output voltage in transient mode considering this converter operating a PV system.

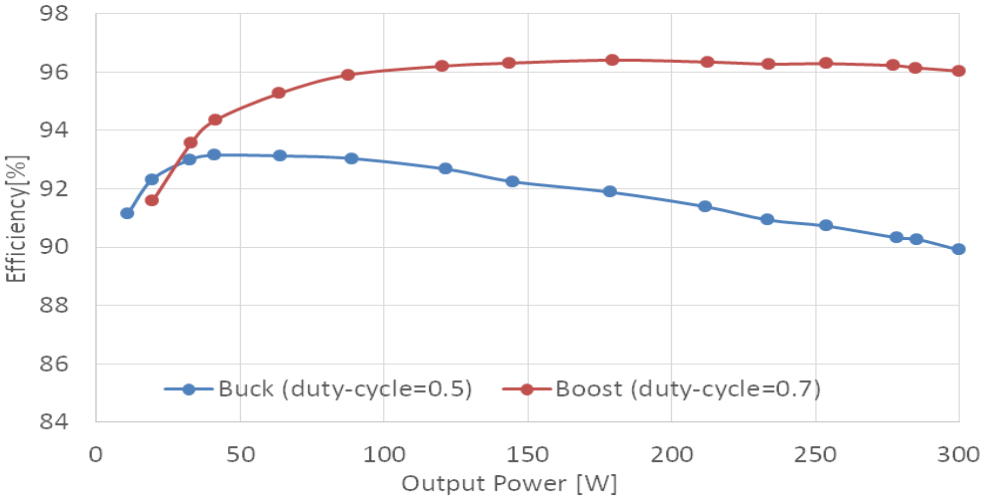

Figure 26. Experimental results regarding the efficiency of the proposed converter operating in buck and boost modes as a function of the output power.

To analyze the converter's efficiency, an analysis of the power-loss breakdown was also conducted, considering the conduction and switching losses of all components. Figure 27 shows the obtained power-loss breakdown, considering diodes, MOSFET, and passive components. On the basis of these results, it can be seen that the losses of the power semiconductors were dominant.

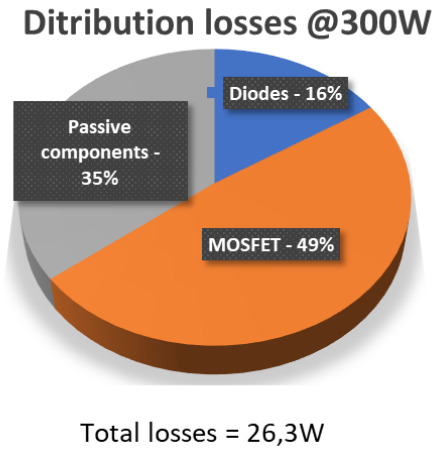

Figure 27. Experimental results for the power-loss breakdown of the converter.

6. Conclusions

In this study, a new topology for a buck-boost DC-DC converter with an extended duty-cycle range in the buck region was proposed. The proposed micro DC-DC converter topology uses a single controlled power switch and is designed to privilege the buck region by extending the range of duty cycles, enabling output voltages smaller than the input voltages, compared to the range in the classic buck-boost converter. This is useful for applications requiring higher definition in low duty cycles. In fact, the proposed converter also enables a reduction of the voltage stress across the controlled power switch and across the diodes. The disadvantage is that the efficiency is in general slightly lower than that of classical converters with buck-boost characteristics. Another aspect is that, in practice, due to the non-ideal nature of the converter's reactive components and the semiconductors, the boost gain is limited, as in many boost converters.

Due to the characteristics of this topology, it can provide an attractive solution for maximum power point tracking in renewable energy resources, in cases where low voltage PVs require a series connection to attain DC output voltages high enough to supply inverters connected to the AC grid. By extending the duty-cycle range in the buck region, the proposed converter enables the design of a series of PV strings with a voltage high enough to supply the AC inverters using moderate duty cycles (0.5–0.7). In the presence of strong variations in irradiance, such as in conditions with shadows, the extended-buck duty cycle range would be useful for precise maximum power point tracking in all series-connected PV panels or for power derating.

Author Contributions: Conceptualization, J.M. and V.F.P.; methodology, J.M. and V.F.P.; software, J.M. and V.F.P.; validation, D.F. and A.C.; formal analysis, J.M. and V.F.P.; investigation, J.M. and V.F.P.; resources, V.F.P., D.F. and A.C.;writing—original draft preparation, J.M.; writing—review and editing, J.M., V.F.P. and J.F.S.; supervision, J.F.S. and S.P.; All authors have read and agreed to the published version of the manuscript.

Funding: This work was supported by national funds through FCT Fundação para a Ciência e a Tecnologia with references PTDC/EEI-EEE/32550/2017, UIDB/50021/2020 and UIDB/00066/2020.

Conflicts of Interest: The authors declare no conflict of interest.

Nomenclature

V_i	input DC voltage to the converter, V
δ	duty cycle
T_s	switching period
L_1, L_2	inductance of inductor(s), Henry
C_1, C_2	capacitance of capacitor(s), Farad
D_1, D_2, D_3	diodes
Δt_1	capacitor discharge time
R_o	load resistance, Ohm
S_w	switch (MOSFET)
V_o	regulated output DC voltage, V
ΔV_{C1}, ΔV_{C2}	peak-to-peak capacitor(s) ripple voltage, V
f	switching frequency, Hz
P_O	output power, W
I_{SW}	RMS switch current, A
ΔQ	charge variation
I_{L1}, I_{L2}	current through inductor(s), A
V_{D1}, V_{D2}, V_{D3}	voltage across the diodes, V
V_T	voltage stress on switch, V

References

1. Hossain, M.Z.; Rahim, N.A.; Selvaraj, J. Recent progress and development on power DC-DC converter topology, control, design and applications: A review. *Renew. Sustain. Energy Rev.* **2018**, *81 Pt 1*, 205–230. [CrossRef]
2. Kjaer, S.B.; Pedersen, J.K.; Blaabjerg, F. Power inverter topologies for photovoltaic modules-a review. In Proceedings of the Conference Record of the 2002 IEEE Industry Applications Conference. 37th IAS Annual Meeting (Cat. No. 02CH37344), Pittsburgh, PA, USA, 13–18 October 2002; Volume 2, pp. 782–788.
3. Murillo-Yarce, D.; Restrepo, C.; Lamar, D.G.; Hernando, M.M.; Sebastián, J. Study of Multiple Discontinuous Conduction Modes in SEPIC, Ćuk, and Zeta Converters. *Electronics* **2022**, *11*, 3744. [CrossRef]
4. Ellabban, O.; Abu-Rub, H.; Blaabjerg, F. Renewable energy resources: Current status, future prospects and their enabling technology. *Renew. Sustain. Energy Rev.* **2014**, *39*, 748–764. [CrossRef]
5. Pires, V.F.; Foito, D.; Cordeiro, A. A DC–DC Converter With Quadratic Gain and Bidirectional Capability for Batteries/Supercapacitors. *IEEE Trans. Ind. Appl.* **2018**, *54*, 274–285. [CrossRef]
6. Hattori, S.; Eto, H.; Kurokawa, F. High Power Density Battery Charger for Plug-In Micro EV. *Int. J. Renew. Energy Res.* **2018**, *8*, 1006–1015.
7. Raghavendra, K.V.G.; Zeb, K.; Muthusamy, A.; Krishna, T.N.V.; Kumar, S.V.S.V.P.; Kim, D.-H.; Kim, M.-S.; Cho, H.-G.; Kim, H.-J. A Comprehensive Review of DC–DC Converter Topologies and Modulation Strategies with Recent Advances in Solar Photovoltaic Systems. *Electronics* **2020**, *9*, 31. [CrossRef]
8. Paragond, L.; Kurian, C.; Singh, B.; Jyothi, A. Simulation and Control of DC/DC Converter for MPPT Based Hybrid PV/Wind Power System. *Int. J. Renew. Energy Res.* **2014**, *4*, 801–809.
9. Tofoli, F.L.; de Castro Pereira, D.; de Paula, W.J.; de Sousa Oliveira Junior, D. Survey on non-isolated high-voltage step-up DC-DC topologies based on the boost converter. *IET Power Electron.* **2015**, *8*, 2044–2057. [CrossRef]
10. Dadras, M.; Farrokhifar, M. A High Performance DC/DC Converter Application to Obtain the Maximum Output Power of Solar Cells. *Int. J. Renew. Energy Res.* **2015**, *5*, 766–772.
11. Williams, B.W. DC-to-DC converters with continuous input and output power. *IEEE Trans. Power Electron.* **2013**, *28*, 2307–2316. [CrossRef]
12. Pires, V.F.; Foito, D.; Silva, J.F. A single switch hybrid DC/DC converter with extended static gain for photovoltaic applications. *Electr. Power Syst. Res.* **2017**, *146*, 228–235. [CrossRef]
13. Kumar, R.; Kannan, R.; Singh, N.S.S.; Abro, G.E.M.; Mathur, N.; Baba, M. An Efficient Design of High Step-Up Switched Z-Source (HS-SZSC) DC-DC Converter for Grid-Connected Inverters. *Electronics* **2022**, *11*, 2440. [CrossRef]
14. Gholizadeh, H.; Ben-Brahim, L. A New Non-Isolated High-Gain Single-Switch DC–DC Converter Topology with a Continuous Input Current. *Electronics* **2022**, *11*, 2900. [CrossRef]
15. Abdullah, A.; Al-Hindaw, M.; Al-Turki, Y.; Mandal, K.; Giaouris, D.; Banerjee, S.; Voutetakis, S.; Papadopoulou, S. Stability of a boost converter fed from photovoltaic source. *Sol. Energy* **2013**, *98 Pt C*, 458–471.
16. Son, H.-S.; Kim, J.-K.; Lee, J.-B.; Moon, S.-S.; Park, J.-H.; Lee, S.-H. A New Buck–Boost Converter With Low-Voltage Stress and Reduced Conducting Components. *IEEE Trans. Ind. Electron.* **2017**, *64*, 7030–7038. [CrossRef]
17. Chen, J.; Maksimovic, D.; Erickson, R.W. Analysis and design of a low-stress buck boost converter in universal-input PFC applications. *IEEE Trans. Power Electron.* **2006**, *21*, 320–329. [CrossRef]

18. Zhang, D.; Chen, D.Y.; Lee, F.C. An experimental comparison of conducted EMI emissions between a zero-voltage transition circuit and a hard-switching circuit. In Proceedings of the PESC Record. 27th Annual IEEE Power Electronics Specialists Conference (PESC'96), Baveno, Italy, 23–27 June 1996; pp. 1992–1997.
19. Kircher, D.; Pommerenke, D.J. EMC Analysis of the Inverting Boost/Buck Converter Topology. *Electronics* **2022**, *11*, 3388. [CrossRef]
20. Li, Q.; Wolfs, P. A Review of the Single Phase Photovoltaic Module Integrated Converter Topologies With Three Different DC Link Configurations. *IEEE Trans. Power Electron.* **2008**, *23*, 1320–1333.
21. Kang, F. Modified multilevel inverter employing half- and full-bridge cells with cascade transformer and its extension to photovoltaic power generation. *Electr. Power Syst. Res.* **2010**, *80*, 1437–1445. [CrossRef]
22. Haroun, R.; El Aroudi, A.; Cid-Pastor, A.; Garcia, G.; Olalla, C.; Martínez-Salamero, L. Impedance Matching in Photovoltaic Systems Using Cascaded Boost Converters and Sliding-Mode Control. *IEEE Trans. Power Electron.* **2015**, *30*, 3185–3199. [CrossRef]
23. Islam, M.; Mekhilef, S. An improved transformerless grid connected photovoltaic inverter with reduced leakage current. *Energy Convers. Manag.* **2014**, *88*, 854–862. [CrossRef]
24. Liu, H.; Li, F.; Ai, J. A Novel High Step-Up Dual Switches Converter With Coupled Inductor and Voltage Multiplier Cell for a Renewable Energy System. *IEEE Trans. Power Electron.* **2016**, *31*, 4974–4983. [CrossRef]
25. Alonge, F.; Busacca, A.; Calabretta, M.; D'Ippolito, F.; Fagiolini, A.; Garraffa, G.; Messina, A.A.; Sferlazza, A.; Stivala, S. Nonlinear Robust Control of a Quadratic Boost Converter in a Wide Operation Range, Based on Extended Linearization Method. *Electronics* **2022**, *11*, 2336. [CrossRef]
26. Zhu, M.; Luo, F.L. Development of Voltage Lift Technique on Double-Output Transformerless DC-DC Converter. In Proceedings of the IECON 2007—33rd Annual Conference of the IEEE Industrial Electronics Society, Taipei, Taiwan, 5–8 November 2007; pp. 1983–1988.
27. Pires, V.; Cordeiro, A.; Foito, D.; Silva, J. High Step-Up DC–DC Converter for Fuel Cell Vehicles Based on Merged Quadratic Boost–Ćuk. *IEEE Trans. Veh. Technol.* **2019**, *68*, 7521–7530. [CrossRef]
28. Haider, Z.; Ulasyar, A.; Khattak, A.; Zad, H.S.; Mohammad, A.; Alahmadi, A.A.; Ullah, N. Development and Analysis of a Novel High-Gain CUK Converter Using Voltage-Multiplier Units. *Electronics* **2022**, *11*, 2766. [CrossRef]
29. Gu, Y.; Li, W.; Zhao, Y.; Yang, B.; Li, C.; He, X. Transformerless Inverter With Virtual DC Bus Concept for Cost-Effective Grid-Connected PV Power Systems. *IEEE Trans. Power Electron.* **2013**, *28*, 793–805. [CrossRef]
30. Azri, M.; Rahim, N.A.; Halim, W.A. A Highly Efficient Single-phase Transformerless H-bridge Inverter for Reducing Leakage Ground Current in Photovoltaic Grid-connected System. *Electr. Power Compon. Syst.* **2015**, *43*, 928–938. [CrossRef]
31. Yu, W.; Lai, J.-S.; Qian, H.; Hutchens, C. High-Efficiency MOSFET Inverter with H6-Type Configuration for Photovoltaic Nonisolated AC-Module Applications. *IEEE Trans. Power Electron.* **2011**, *26*, 1253–1260. [CrossRef]
32. Rosas-Caro, J.C.; Ramirez, J.M.; Peng, F.Z.; Valderrabano, A. A DC-DC multilevel boost converter. *IET Power Electron.* **2010**, *3*, 129–137. [CrossRef]
33. Addula, S.R.; Mahalingam, P. Coupled Inductor Based Soft Switched Interleaved DC-DC Converter for PV Applications. *Int. J. Renew. Energy Res.* **2016**, *6*, 361–374.
34. Ravyts, S.; Vecchia, M.D.; Zwysen, J.; Van den Broeck, G.; Driesen, J. Study on a cascaded DC-DC converter for use in building-integrated photovoltaics. In Proceedings of the 2018 IEEE Texas Power and Energy Conference (TPEC), College Station, TX, USA, 8–9 February 2018.
35. Mitsui, K.; Sato, T.; Nishijima, K.; Nabeshima, T. LLC converter combined with switched capacitor for high voltage applications. In Proceedings of the 2013 International Conference on Renewable Energy Research and Applications (ICRERA), Madrid, Spain, 20–23 October 2013; pp. 1013–1017.
36. Liu, H.; Hu, H.; Wu, H.; Xing, Y.; Batarseh, I. Overview of High-Step-Up Coupled-Inductor Boost Converters. *IEEE J. Emerg. Sel. Top. Power Electron.* **2016**, *4*, 689–704. [CrossRef]
37. Pires, V.F.; Foito, D.; Cordeiro, A.; Silva, J.F. A Single-Switch DC/DC Buck-Boost Converter with Extended Output Voltage. In Proceedings of the 7th International Conference on Renewable Energy Research and Applications (ICRERA), Paris, France, 14–17 October 2018; pp. 791–796. [CrossRef]
38. Seguel, J.L.; Seleme, S.I., Jr.; Morais, L.M.F. Comparative Study of Buck-Boost, SEPIC, Cuk and Zeta DC-DC Converters Using Different MPPT Methods for Photovoltaic Applications. *Energies* **2022**, *15*, 7936. [CrossRef]
39. Kano, F.; Kasai, Y.; Kimura, H.; Sagawa, K.; Haruna, J.; Funato, H. Buck-Boost-Type MPPT Circuit Suitable for Vehicle-Mounted Photovoltaic Power Generation. *IEEJ Trans. Electr. Electron. Eng.* **2021**, *16*, 1229–1238. [CrossRef]
40. Shaw, P.; Siddique, M.D.; Mekhilef, S.; Iqbal, A. A new family of high gain boost DC-DC converters with reduced switch volt-age stress for renewable energy sources. *Int. J. Circ. Theor. Appl.* **2022**, 1–21. [CrossRef]
41. Khubchandani, V.; Veerachary, M. Extended Bucking Range Fifth-Order Buck-Boost Converter. In Proceedings of the IEEE International Conference on Power Electronics, Drives and Energy Systems (PEDES), Jaipur, India, 16–19 December 2020; pp. 1–6. [CrossRef]
42. Mashinchi Maheri, H.; Vinnikov, D.; Chub, A.; Sidorov, V.; Liivik, E. Impact of Transformer Turns Ratio on the Power Losses and Efficiency of the Wide Range Isolated Buck–Boost Converter for Photovoltaic Applications. *Energies* **2020**, *13*, 5645. [CrossRef]
43. Zhang, G.; Yuan, J.; Yu, S.S.; Zhang, N.; Wang, Y.; Zhang, Y. Advanced four-mode-modulation-based four-switch non-inverting buck–boost converter with extra operation zone. *IET Power Electron.* **2020**, *13*, 2049–2059. [CrossRef]

44. Mahmood, A.; Zaid, M.; Ahmad, J.; Khan, M.A.; Khan, S.; Sifat, Z.; Lin, C.H.; Sarwar, A.; Tariq, M.; Alamri, B. A Non-Inverting High Gain DC-DC Converter with Continuous Input Current. *IEEE Access* **2021**, *9*, 54710–54721. [CrossRef]
45. Bertoluzzo, M.; Bignucolo, F.; Bullo, M.; Diantini, M.; Dughiero, F.; Lancerin, M.; Sieni, E.; Vinante, M.; Zordan, M. A buck-boost DC-DC converter for single module photovoltaic application to vehicle recharge. In Proceedings of the IEEE 19th Workshop on Control and Modeling for Power Electronics (COMPEL), Padua, Italy, 25–28 June 2018; pp. 1–6. [CrossRef]
46. Sarwar, S.; Javed, M.Y.; Jaffery, M.H.; Ashraf, M.S.; Naveed, M.T.; Hafeez, M.A. Modular Level Power Electronics (MLPE) Based Distributed PV System for Partial Shaded Conditions. *Energies* **2022**, *15*, 4797. [CrossRef]
47. Ahmad, J.; Sidique, M.; Sarwar, A.; Lin, C.; Iqbal, A. A high gain noninverting DC–DC converter with low voltage stress for industrial applications. *Int. J. Circuit Theory Appl.* **2021**, *49*, 4212–4230. [CrossRef]
48. Abdel-Rahim, O.; Chub, A.; Blinov, A.; Vinnikov, D. New High-Gain Non-Inverting Buck-Boost Converter. In Proceedings of the IECON 2021—47th Annual Conference of the IEEE Industrial Electronics Society, Toronto, ON, Canada, 13–16 October 2021; pp. 1–6. [CrossRef]